Environmental Science & Technology

Article

Cite This: Environ. Sci. Technol. 2018, 52, 13202−13211

pubs.acs.org/est

Effect of Manganese Oxide Aging and Structure Transformation on the Kinetics of Thiol Oxidation

Eryn M. Eitel, Shiliang Zhao, Yuanzhi Tang, and Martial Taillefert*

School of Earth and Atmospheric Sciences, Georgia Institute of Technology, Atlanta, Georgia 30332-0340, United States

Supporting Information

ABSTRACT: The kinetics and mechanism of thiol oxidation by Mn oxides undergoing dynamic structural transformation under environmentally relevant conditions remain poorly understood. In this study, thiol/disulfide pair concentrations were simultaneously determined in situ using voltammetric microelectrodes during the interaction of four common thiols (cysteine, homocysteine, cysteamine, and glutathione) with fresh and aged δ-MnO_2 at pH 7.0. The reaction kinetics was first order with respect to thiol and zero order with respect to Mn oxides. A transient intermediate sulfur surface species observed during the reaction provides evidence for a mechanism involving two successive one-electron transfer steps. The reaction kinetics of fresh and aged δ-MnO_2 was investigated with cysteine and compared to that of manganite, a Mn(III) oxyhydroxide phase. The reactivity of aged δ-MnO_2 decreased as a result of structural transformation to cryptomelane but remained higher than that of manganite, suggesting the potential roles of transient Mn(III) surface intermediate in promoting the reduction of Mn(IV) in δ-MnO_2 and cryptomelane (compared to Mn(III) in manganite). This study demonstrates the importance of correlating Mn oxide mineral structure and redox reactivity and extends the potential for thiols commonly found in sedimentary environments to be utilized as electron shuttles during dissimilatory Mn reduction.

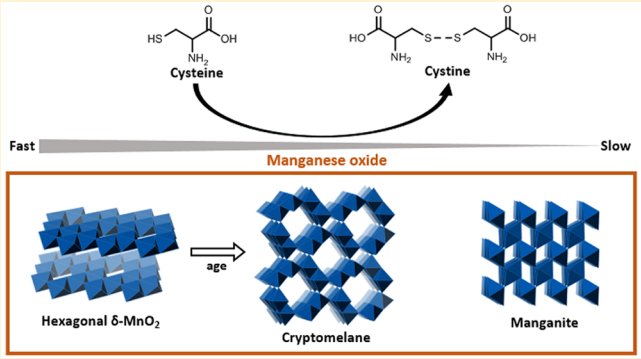

1. INTRODUCTION

Manganese (Mn) is the second most prevalent transition metal in Earth's crust after iron (Fe) and plays important roles in the biogeochemical cycling of carbon, nitrogen, phosphorus, sulfur, and iron in sediments.[1−6] The transformation of Mn(III,IV) (oxyhydr)oxides (hereafter referred to as Mn oxides) also influences the transport and fate of inorganic (e.g., refs 7−11) and organic[12] contaminants. Both layered and tunnel structured Mn oxides are commonly found in natural environments.[13,14] Fresh biogenic Mn oxides are typically highly reactive layered hexagonal phyllomanganates that are structurally similar to δ-MnO_2 (vernadite) and birnessite, and have high surface area and a large number of vacancy sites.[4,15,16] Although layered phyllomanganates are typically more abundant,[16] 2 × 2 tunnel structured hollandite type Mn oxides (such as cryptomelane) represent the major phases detected in the supergene oxidation zones of Mn deposits and lateritic weathered profiles.[17−20] In marine sediments, aged Mn(III,IV) oxides with higher structure order and lower reactivity as well as Mn(III) oxyhydroxides (such as manganite with 1 × 1 tunnel structure) dominate the oxic layers closest to the sediment−water interface.[21,22] Indeed, dissolved Mn(II) is known to react with structural Mn(IV) in Mn(III,IV) oxides to produce Mn(III) and result in phase transformations. Low Mn(II) concentrations may favor the transformation of birnessite layer symmetry from hexagonal to triclinic (e.g., refs 23−25). At higher Mn(II) concentration and under anoxic conditions, such reductive transformation can lead to the formation of manganite (γ-$Mn^{III}OOH$) at pH 7.0−8.0 and hausmannite ($Mn^{II}Mn^{III}{}_2O_4$) at pH 8.0−8.5.[26,27] Under oxic conditions, reaction of concentrated Mn(II) with hexagonal birnessite was found to generate cryptomelane ($K_{1.3-1.5}Mn^{III,IV}{}_8O_{16}$) at pH 4.0, groutite ($\alpha$-MnOOH) at pH 6.0, and manganite at pH 7−7.5.[28,29] Wet−dry cycling has been reported to facilitate the conversion of birnessite into tunneled Mn oxides in freshwater sediments.[30]

As a result of the variety of processes affecting Mn oxide formation, structure, and transformation, the redox reactivity of Mn oxides in natural sediments varies widely.[22] Both the chemical[12] and microbial[31] reduction of disordered low crystallinity Mn oxides, which have higher surface area and more reactive vacancy sites, are faster than the higher crystallinity phases. As microorganisms may recycle electron shuttling compounds to reduce solid metal oxides,[32−34] the abiotic oxidation of these electron shuttles may be affected by differences in mineral structure. Thiols represent excellent electron shuttles for the dissimilatory reduction of Fe(III)-

Received: July 19, 2018
Revised: September 26, 2018
Accepted: October 25, 2018
Published: October 25, 2018

DOI: 10.1021/acs.est.8b03993
Environ. Sci. Technol. 2018, 52, 13202−13211

containing minerals such as poorly crystalline Fe(III) oxides[35] and smectite[36] and are likely to be utilized during dissimilatory Mn reduction. The overall reduction of Mn(IV) by thiols (RSH) produces one mole of Mn(II) and disulfide species (RSSR) per two moles of thiol reactant (eq 1):

$$MnO_2 + 2RSH + 2H^+ \leftrightarrow RSSR + Mn^{2+} + 2H_2O \quad (1)$$

Although the kinetics of Fe oxide reduction by different thiols has been extensively studied,[37,38] investigations of the reaction of thiols with solid Mn oxides have been limited and require analytical techniques that are capable of probing the fast reaction kinetics and related structural changes during the reaction.[39−42]

The reaction between Mn oxides and thiols is of interest as it likely influences Mn redox cycling, the mobilization and redox transformation of inorganic and organic contaminants, and a number of biogeochemical processes affected by Mn transformations. This study systematically investigated the reaction kinetics of four low molecular weight thiols (cysteamine, cysteine, homocysteine, and reduced glutathione) with environmentally common Mn oxide phases, including δ-MnO_2 of different ages/structure and manganite, to examine the effects of aging and phase transformation on reaction kinetics. To the best of our knowledge, this is the first study that determines the kinetic of solid Mn oxide reaction with thiols under environmentally relevant conditions.

2. MATERIALS AND METHODS

Materials and Solid Phase Characterization. Unless otherwise stated, all chemicals were at least ACS grade reagents and obtained from Sigma-Aldrich, Inc. Stock solutions of thiol and disulfide were prepared weekly and stored at 4 °C. δ-MnO_2 was prepared by the oxidation of Mn(II) by permanganate following a previous procedure.[43] Aging and low temperature transformation of δ-MnO_2 were allowed to occur in the original synthesis solution containing excess K^+.[44] At varied time points (1 month to 6 years), aliquots of the aging suspension were removed, repeatedly rinsed, and resuspended in the reaction medium. These samples are labeled as δ-MnO_2_aging time (e.g., δ-MnO_2_1m and δ-MnO_2_2yr indicates δ-MnO_2 samples aged for 1 month and 2 years). Cryptomelane was prepared by the addition of heated potassium permanganate solution to manganese sulfate solution.[45,46] manganite was synthesized by reacting 36 mM Mn(II) with 1 g/L δ-MnO_2 under anoxic conditions for 3 months at pH 7.[47] A portion of the synthesized solid phases were freeze-dried and characterized by X-ray diffraction (XRD) using a Panalytical Empyrean diffractometer with Cu Kα radiation (λ = 0.15406 nm) and by Mn K-edge X-ray absorption spectroscopy (XAS) (details in Supporting Information (SI) Text S1). Surface area of the Mn oxides was determined by nitrogen physiosorption at 77 K using the BET method on a Micromeritics TriStar 2030 after vacuum drying for 12 h at room temperature.

Experimental Setup. Experiments were performed at room temperature in a DLK Cell Stand (Analytical Instruments System Inc.) specifically fabricated for use with gold/mercury amalgam (Au/Hg) voltammetric microelectrodes. Reactor cells were amended with Mn oxide suspensions and degassed for 10 min using ultrahigh purity (UHP) N_2. Thiols were injected to initiate the reaction, and the suspension was constantly stirred during the experiments, except during the voltammetric analyses (<20 s). All experiments were conducted in at least duplicate in solution composed of inorganic salts (mainly $(NH_4)_2SO_4$) buffered at pH 7.0 with 5.7 mM K_2HPO_4/ 3.3 mM KH_2PO_4 (0.09 M ionic strength).[48] The phosphate buffer had no effect on thiol oxidation as determined in otherwise identical experiments conducted with PIPES buffer (SI Text S2 and Figure S1). In addition, disulfide products were not detected in control experiments without δ-MnO_2. In independent experiments, cysteine and homocysteine concentrations varied between 300 and 1000 μM in the presence of 10 mM δ-MnO_2 aged for 1.5 or 2.5 years, whereas concentrations of δ-MnO_2 aged for 1.5 years varied between 5 and 15 mM in the presence of 500 μM cysteine to determine the reaction order with respect to each species.

In Situ Electrochemical Thiol and Disulfide Measurements. In situ voltammetric measurements of thiol and disulfide species in the thiol-Mn oxide reaction suspension were performed according to previous procedures[38] with a three electrode system consisting of a 100 μm diameter Au/Hg microelectrode as working electrode, a 500 Pt μm diameter counter electrode, and a 500 μm diameter Ag/AgCl reference electrode all encased in 3 mm diameter PEEK (polyethyl etherketone) tubing as previously described.[49] All the potentials reported in this study are therefore relative to the standard potential of the saturated Ag/AgCl system. The Au/Hg microelectrode was prepared by polishing the gold wire with 15, 6, 1, and 0.25 μm diamond pastes (Buehler) followed by plating with Hg at −0.1 V in a $Hg(NO_3)_2$ solution for 4 min and polarization at −9.0 V for 90 s to stabilize the amalgam.[50] Voltammetric measurements were carried out with a computer-operated DLK-100 potentiostat (Analytical Instrument Systems, Inc.), and data was integrated using VOLTINT a semiautomated Matlab script.[51] To confirm electrode quality, linear sweep voltammograms of dissolved oxygen and Mn(II) calibrations were obtained.[49] The electrodes were then calibrated for thiols and disulfide species in degassed solution.

3. RESULTS AND DISCUSSION

Effect of Aging on the Structural Transformation of δ-MnO_2. Long-term aging of fresh δ-MnO_2 led to the formation of cryptomelane as a final product, as evident in the XRD patterns of fresh and aged δ-MnO_2 (Figure 1). Similar transformation have been previously observed in suspensions of birnessite over time at room temperature.[52] XRD data of the fresh δ-MnO_2 is consistent with previous studies, with two broad peaks at ∼37° (11,20) and ∼66° (31,02). The very weak peak at ∼25° (002) indicates limited layer stacking along the *c* axis. Upon aging, the peaks at ∼22°, 43°, and 57° first increased then decreased. These peaks indicate the formation of phyllomanganate phase/sheets with orthogonal (triclinic) symmetry,[53−55] which is a common transformation product upon Mn oxide interaction with low concentrations of dissolved Mn(II).[23,24,53,56−58] In addition, XRD peaks (at ∼18°, 29°, 38°, 42°, 50°) corresponding to cryptomelane (a 2 × 2 tunnel structured tectomanganate phase) continuously increased after ∼1 month of the aging process, and cryptomelane was the only phase observed after 6 years of aging time (sample δ-MnO_2_6year in Figure 1), suggesting that the triclinic phyllomanganate phase served as an intermediate during the transformation from δ-MnO_2 to cryptomelane. Presence of intermediate triclinic phyllomanganates were also observed in previous studies during Mn oxide transformation from layered to tunneled structure.[59,60] Mn(III) in triclinic vernadite sheets is thought to generate a Jahn−

DOI: 10.1021/acs.est.8b03993
Environ. Sci. Technol. 2018, 52, 13202−13211

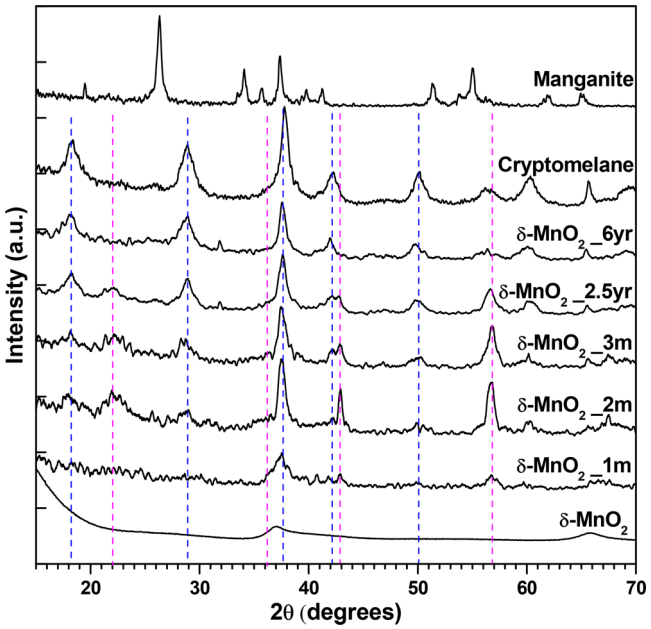

Figure 1. XRD patterns of manganite, cryptomelane, fresh δ-MnO_2, and δ-MnO_2 aged for 1 month, 2 months, 3 months, 2.5 years, and 6 years. Blue and magenta vertical dashed lines indicate peaks corresponding to cryptomelane and triclinic birnessite, respectively.

Teller effect that promotes the transition from layered to tunneled structure.[61]

Figure S2 and S3 show the k^3-weighted Mn K-edge extended X-ray absorption fine structure (EXAFS) and X-ray absorption near edge structure (XANES) data of fresh and aged δ-MnO_2, as well as cryptomelane and triclinic birnessite. XANES data confirm the oxidation state of the different δ-MnO_2 synthesized. The gradual transformation from δ-MnO_2 to cryptomelane is clearly observed from the changes in the ~7.5−10 $Å^{-1}$ indicator region of the EXAFS spectra. Linear combination fitting (LCF) using fresh δ-MnO_2, cryptomelane, and triclinic birnessite as end members (SI Table S1) indicates the presence of ~51% δ-MnO_2, ~9% triclinic birnessite, and ~41% cryptomelane in the 1-month-old sample (δ-MnO_2_1m), and almost complete transformation to cryptomelane after 2.5 years (samples δ-MnO_2_2.5yr and δ-MnO_2_6yr). Interestingly, the LCF obtained fraction of triclinic birnessite was lower than expected, whereas that of cryptomelane was higher than expected from XRD data (Figure 1). These differences may be due to analytical limitations of these two spectroscopic techniques. XRD detects the long-range structural order, therefore better ordered (i.e., higher crystallinity) phases display more distinctive peaks (in this case triclinic birnessite and cryptomelane) than poorly ordered (i.e., low crystallinity) phases (in this case the broad peaks corresponding to hexagonal δ-MnO_2). In comparison, XAS is an element specific technique that probes local coordination environment around the central atom (in this case Mn) but does not discriminate phases of varying crystallinity. Despite variations in the relative abundance of the different Mn phases obtained from XRD and XAS analysis, the overall trend in the aging system is consistent with the gradual disappearance of hexagonal δ-MnO_2, formation of a triclinic birnessite intermediate phase, and the ultimate conversion to cryptomelane. The above-mentioned changes in Mn-containing phase and crystallinity are also consistent with the gradual decrease of BET specific surface area observed with age (SI Table S2).

Effect of Thiol Structure on Thiol Oxidation Kinetics. To examine the relative reactivity of different thiols, cysteamine, cysteine, homocysteine, and reduced glutathione were

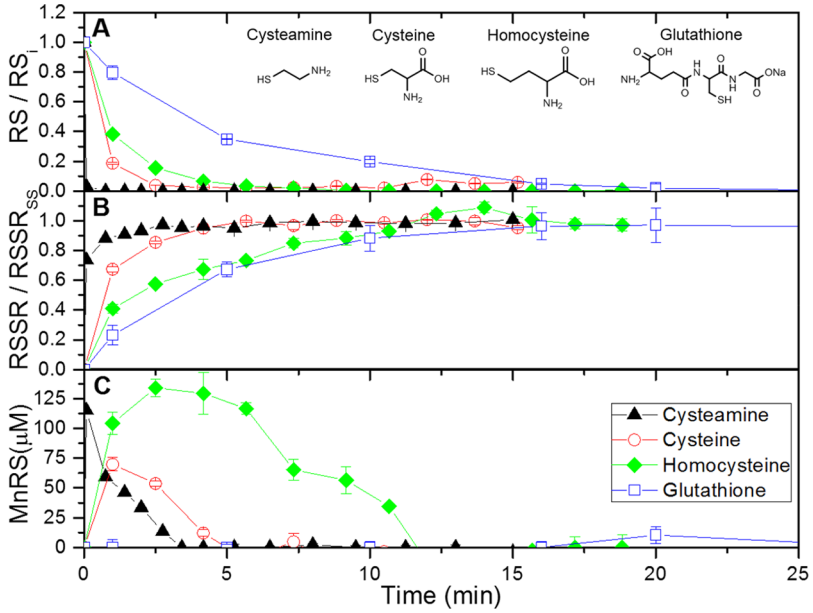

Figure 2. Temporal evolution of (A) thiol (RS) concentration normalized to the initial thiol concentration (RS_i) of cysteamine (CA), cysteine (CS), homocysteine (HS), and reduced glutathione (GS); (B) the disulfide product (RSSR) concentration normalized to the disulfide concentration at steady state ($RSSR_{SS}$) of cystamine (CAAC), cystine (CSSC), homocystine (HSSH), and oxidized glutathione (GSSG); and (C) the intermediate sulfur surface species (MnRS) calculated from mass balance during the reaction of 500 μM thiol with 10 mM δ-MnO_2 aged for 1.5 years at pH 7.0. Standard deviations represent the average of at least triplicate measurements at each time point and are often smaller than the symbols.

DOI: 10.1021/acs.est.8b03993
Environ. Sci. Technol. 2018, 52, 13202−13211

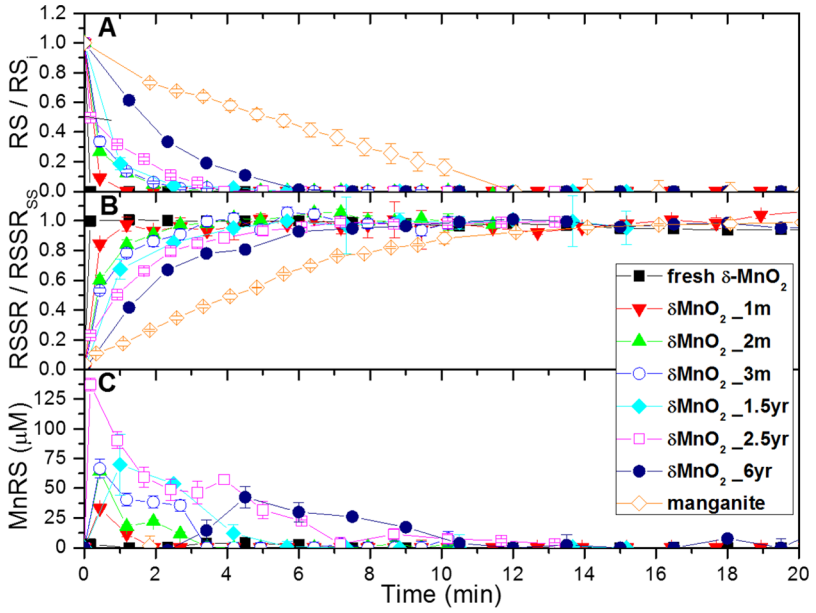

Figure 3. Temporal evolution of (A) the cysteine (CS) reactant normalized to the initial concentration of cysteine (RS/RS_i), (B) the cystine product (CSSC) normalized to the cystine concentration at steady state ($RSSR/RSSR_{SS}$), and (C) the intermediate sulfur surface species (MnRS) calculated from mass balance in solution during the reaction of 500 μM cysteine with 10 mM δ-MnO_2 of different age or 10 mM manganite at pH 7.0. Standard deviations represent the average of at least triplicate measurements at each time point and are often smaller than the symbols.

reacted with 1.5-year-old δ-MnO_2 (δ-MnO_2_1.5yr). All thiols were rapidly oxidized and the resulting disulfide product was simultaneously released into solution (Figure 2A, B). However, clear differences in the reaction kinetics were observed between the thiols: Cysteamine reacted the fastest and was completely removed from solution within the first minute (half-life <10 s), followed by cysteine, homocysteine, and reduced glutathione, which were removed with half-lives of 1.75, 2, and 4.5 min, respectively. The formation kinetics of the disulfide product followed the order of disappearance of their corresponding thiol: Cystamine reached equilibrium concentrations after 2.5 min, followed by cystine (4 min), homocystine (12.5 min), and oxidized glutathione (16 min). In general, the reaction rates of thiols with Mn oxides were significantly higher than the previously reported reaction rates of thiols with ferrihydrite under identical conditions.[38] Reactions between cysteamine and 1.5-year-old δ-MnO_2 resulted in a half-life 33 times shorter than that of cysteamine reaction with ferrihydrite. Similarly, half-lives of cysteine, homocysteine, and glutathione reacted with 1.5-year-old δ-MnO_2 were 8.6, 16, and 13.6 times shorter than those reacted with ferrihydrite.[38] These findings are consistent with the differences in reactivity of Fe(III) and Mn(IV) molecular orbitals with dissolved sulfide[62] and the lower redox potential of Fe(III) oxides.[63] Similar results have been observed with birnessite, cryptomelane, and Fe(III) oxides during the oxidation of phenolic compounds.[64] The reactivity of the different thiols followed the same trend as observed with ferrihydrite[38] and agreed with results obtained with MnO_2 nanoparticles.[40] In contrast to the ferrihydrite system,[38] however, the conversion of thiols to their respective disulfide product was complete as theoretical concentrations of disulfide were always reached at steady state (Figure 2B).

The simultaneous analysis of both the thiol reactant and disulfide product in solution by voltammetric microelectrodes over such a short time scale is unique and allows to close mass balance on the sulfur species. Mass balance calculations (eq 2) can be used to identify any intermediate sulfur surface species (MnRS) formed during the reaction.

$$[\mathrm{MnRS}] = [\mathrm{RS^-}]_0 - [\mathrm{RS^-}] - 2[\mathrm{RSSR}] \quad (2)$$

where $[RS^-]_0$ is the initial concentration of thiol, and $[RS^-]$ and [RSSR] represent the concentrations of dissolved thiol and disulfide measured as a function of time (Figure 2A,B). Although differentiation between surface species cannot be accounted for electrochemically, these calculations indicate that the lifetime of the intermediate sulfur surface complex depends on the thiol structure, as the rate of formation and transformation of the intermediate sulfur complexes with the different thiols decreased in the order of cysteamine > cysteine > homocysteine and was below detection limit over the course of the reaction with glutathione (Figure 2C). The absence of surface-bound glutathione was not unexpected based on its numerous negatively charged functional groups and the increased steric hindrance resulting from the large structure of glutathione compared to the other smaller thiols. Lack of permanently adsorbed glutathione was also observed during reactions with Fe(III) oxides in contrast to similar experiments with cysteamine, cysteine, and homocysteine.[38] The desorption of glutathione here was likely rapid due to the lower point of zero charge (PZC) of Mn(IV) oxides compared to Fe(III) oxides, which decreases the interaction between the negatively charged carboxylic functional groups of the thiol reactant with the negatively charged Mn oxide surface and thus promotes desorption of the product of the reaction once it is formed. In contrast, the high reactivity of cysteamine can be explained by its small size and lack of carboxylic group to interfere with the negative surface charges of the Mn oxide.

Effect of Mn Oxide Aging and Structural Transformation on Thiol Oxidation Kinetics. The reaction between cysteine and fresh δ-MnO_2 was extremely fast and complete almost immediately (Figure 3A), including production of cystine to equilibrium concentrations within the first 15 s (half-life of <6 s, Figure 3B). The reaction rate decreased

DOI: 10.1021/acs.est.8b03993
Environ. Sci. Technol. 2018, 52, 13202−13211

progressively with δ-MnO_2 that was aged for 1 and 2 months (half-lives of 15 and 18 s, respectively), whereas the rate of cysteine oxidation with δ-MnO_2 aged for 2 months, 3 months, and 1.5 years showed no significant difference. With more aged δ-MnO_2 (2.5 and 6 years old), the rate of cysteine oxidation decreased progressively (Figure 3A), likely due to the increased fraction of tunnel structured cryptomelane as identified by XRD and XAS (Figure 1 and SI Figure S2). Meanwhile, the rate of cystine production declined concomitantly, and cystine concentration reached equilibrium within 1, 3, 3.5, 4.25, 7, and 10 min as the age of δ-MnO_2 increased from 1 month to 6 years (Figure 3B). The lowest reaction rates were observed with manganite, which did not reach equilibrium until 14 min (half-life of 5.75 min). For all aged δ-MnO_2 as well as manganite, the concentration of the intermediate sulfur surface complex calculated from mass balance (eq 2) confirmed complete transformation of the thiol to its disulfide product within 15 min. The concentration of the intermediate surface complex with most of the aged δ-MnO_2 reached a maximum within a minute, except for 6-year-old δ-MnO_2 which reached a maximum between 4−5 min (Figure 3C). These results demonstrate that the transformation from layered δ-MnO_2 to tunneled cryptomelane significantly slowed down the reaction.

Mechanism of Thiol Oxidation by Mn Oxides. The mechanism of the reaction has been proposed to proceed via initial adsorption of the electron transferring sulfhydryl group of the thiol onto the Mn(IV)-oxide surface to form a neutral species and a water molecule[40] (eq 3).

$$\equiv Mn(IV)OH + RSH \leftrightarrow \equiv Mn(IV)SR + H_2O \quad (3)$$

The surface species undergoes a series of reactions characterized primarily by a single electron transfer between the sulfur and Mn(IV) center (eq 4) followed by rapid dissolution of the thiol radical (eq 5), adsorption of a second thiol to the surface-bound Mn(III) (eq 6), a second electron transfer (eq 7), and release of the second thiol radical and generation of a surface-bound Mn(II) (eq 8) that is eventually released in solution (eq 9). In solution, the thiol radical immediately dimerizes to form the stable disulfide product (eq 10).

$$\equiv Mn(IV)SR \xrightarrow{e^- \text{transfer}} \equiv Mn(III)SR \quad (4)$$

$$\equiv Mn(III)SR + H_2O \xrightarrow{\text{fast}} \equiv Mn(III)OH + RS^{\cdot} + H^+ \quad (5)$$

$$\equiv Mn(III)OH + RSH \xrightarrow{\text{fast}} \equiv Mn(III)SR + H_2O \quad (6)$$

$$\equiv Mn(III)SR \xrightarrow{e^- \text{transfer}} \equiv Mn(II)SR \quad (7)$$

$$\equiv Mn(II)SR + H_2O \xrightarrow{\text{fast}} \equiv Mn(II)OH_2^+ + RS^{\cdot} \quad (8)$$

$$\equiv Mn(II)OH_2^+ \xrightarrow{\text{fast}} \equiv Mn(IV)OH + Mn(II)_{aq} + H^+ \quad (9)$$

$$2RS^{\cdot} \xrightarrow{\text{fast}} RSSR \quad (10)$$

Based on molecular orbital theory, two separate one-electron transfers and formation of an Mn(III) intermediate is the most probable pathway for reduction of Mn(IV) to Mn(II).[65] Indeed, adsorbed Mn(III) has been identified as intermediate species during the reaction between birnessite and inorganic reductants such as arsenite, Cr(III), and selenite,[66−68] and the microbial reduction of Mn(IV) oxides generates Mn(III) complexes in solution.[69] The reduction of Mn(III) by thiols is not inhibited by common Mn(III) stabilizers, such as pyrophosphate,[70] and the reaction proceeds extremely rapidly (data not shown). As a result, direct detection of a Mn(III) intermediate during thiol oxidation has thus far not been possible.[40] Although electrochemical data cannot identify the intermediate sulfur surface species, mass balance calculations (eq 2) provide novel insights into the reaction mechanism. With cysteamine, homocysteine, and possibly cysteine, a secondary maximum in the concentration of the intermediate sulfur surface species was observed during reaction with the 1.5 year-old δ-MnO_2 (Figure 2C). This secondary maximum in the sulfur intermediate was clearly observed during reaction between cysteine and all δ-MnO_2 aged for more than 1 month (Figure 3C). The presence of the two local maxima in intermediate sulfur surface species suggests that the transformation from layered δ-MnO_2 to tunneled cryptomelane slows down the reaction enough to identify the intermediate sulfur surface species as the Mn(IV) (eq 3) and the Mn(III) (eq 6) thiol complexes formed prior to each electron transfer step. These findings therefore provide evidence for the proposed two steps of one electron transfer from Mn(IV) to Mn(III), and from Mn(III) to Mn(II). As formation of Mn(III) at the surface of the Mn(IV) oxides during the reaction (eq 6) may result in Jahn−Teller distortion which promotes the subsequent reduction of Mn(III) sites,[71] it is likely that the two thiol oxidation reactions proceed at a single site rather than different Mn(IV) centers in these minerals.

Overall Rate Law. From eq 1, the rate of disulfide production at constant pH depends on the concentrations of thiol and Mn oxide, resulting in an experimental rate law that can be generally expressed as

$$R = \frac{d[RSSR]}{dt} = -\frac{1}{2}\frac{d[RS^-]}{dt} = k[RS^-]^a[\text{Mn oxide}]^b \quad (11)$$

where k is the overall rate constant and a and b represent the order of the reaction with respect to each constituent. In the presence of excess Mn oxide, the rate of disulfide production is simplified into a pseudo-order kinetic model as

$$R_i = k_{obs}[RS^-]^a \quad (12)$$

where

$$k_{obs} = k[\text{Mn oxide}]^b \quad (13)$$

is the apparent rate constant. From eq 12, the order of the reaction with respect to the thiol species can be determined as the slope of the linear regression that fits the log of the initial rate of disulfide production as a function of the log of the initial concentration of thiol. By calculating initial rates using the change in disulfide concentration as a function of time during the first 10−15% of the reaction extent, a slope of 0.96 ± 0.07 was determined for the reaction between cysteine and 1,5-year-old δ-MnO_2 (Figure 4), demonstrating first order kinetics with respect to thiol. First order kinetics with respect to thiol was also confirmed for homocysteine reaction with 1,5-year-old δ-MnO_2(slope = 0.91 ± 0.21) and for cysteine reaction with 2,5-year-old δ-MnO_2 (slope = 0.93 ± 0.08) (Figure 4).

Experiments were also conducted with constant cysteine concentrations and varied concentrations of 1.5-year-old δ-MnO_2 to determine k_{obs} at each Mn oxide concentration after integration of eq 12 (with $a = 1$) by representing the natural log of the cysteine concentration ($[RS^-]$) as a function of time (eq 14).

DOI: 10.1021/acs.est.8b03993
Environ. Sci. Technol. 2018, 52, 13202−13211

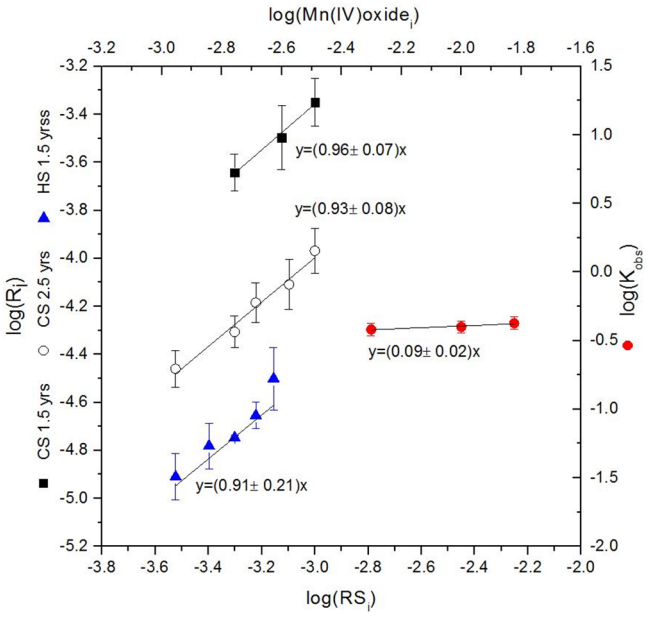

Figure 4. Experimental determination of the reaction order with respect to (left axis) cysteine (CS) and homocysteine (HS) using the isolation method in the presence of 10 mM δ-MnO_2 aged for 1.5 and 2.5 years at pH 7; and (right axis) Mn oxide using the isolation and pseudo-order methods. To determine the order with respect to the Mn oxide, the initial concentration of a suspension of δ-MnO_2 aged for 1.5 years was varied between 5 and 15 mM in a suite of experiments conducted with 500 μM cysteine at pH 7.0.

$$\ln([RS^-]) = -2k_{obs}t + \ln([RS^-]_0) \quad (14)$$

The order of the reaction with respect to Mn oxide (b) was then determined from the slope of the linear regression of the log of k_{obs} as a function of the log of Mn oxide concentration (eq 13). A slope of 0.09 ± 0.02 was determined (Figure 4), indicating a zero order rate law with respect to Mn oxide concentration, as observed previously for the reaction of cysteine with excess MnO_2 nanoparticles[41] and excess Fe(III) oxides.[38]

As a result, the overall kinetic rate law of cysteine oxidation by Mn oxides in environmentally relevant conditions at pH 7 and in the presence of excess Mn oxides can be written as the following first order rate law:

$$R = k[RS^-] \quad (15)$$

Assuming the rate law derived from experiments with cysteine, homocysteine, and two different aged δ-MnO_2 is the same for all thiols and all Mn oxides used in this study, the experimental rate constant (k) can be obtained after integration of the overall first order rate law (eq 15) from the slope of the natural log of the thiol concentration as a function of time normalized to its initial concentration (eq 16) and represented graphically (Figure 5).

$$\ln\left(\frac{[RS^-]}{[RS^-]_0}\right) = -2k \times t \quad (16)$$

The good linearity of the integrated rate law with all thiols (Figure 5A) and the different minerals (Figure 5B) confirms that the overall rate law is accurate. As previously observed with Fe(III) oxides,[38] rate constants decreased in the order of cysteamine > cysteine > homocysteine > glutatione (Figure 6A) as the chemical structure of the reductant increased in

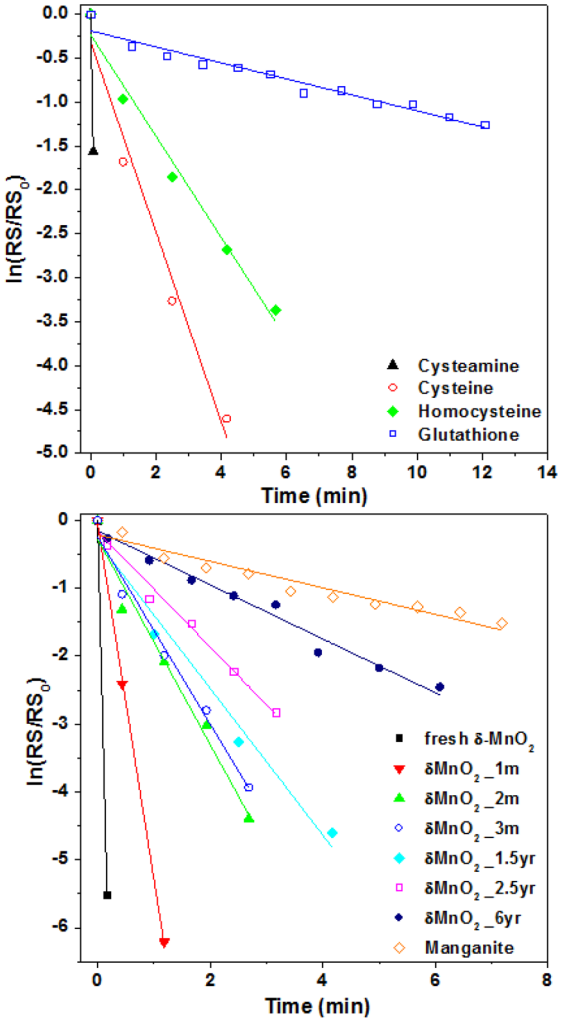

Figure 5. Temporal evolution of the natural logarithmic of the concentration of (A) cysteamine, cysteine, homocysteine, and glutathione normalized to their initial concentration during the reaction of each thiol with 10 mM δ-MnO_2 aged for 1.5 year at pH 7.0; and (B) cysteine normalized to its initial concentration during its oxidation by different age δ-MnO_2 and manganite. The slope of duplicate linear curves was averaged and used to calculate the overall rate constant of the reaction.

complexity. In addition, rate constants decreased with increasing age of δ-MnO_2 (Figure 6B). This decrease was drastic within the first two months of aging then gradual between 3 months and 6 years, even after normalizing the rate constant by the specific surface area (SI Text S3 and Table S2). As rate constants are independent of reactant concentrations and these experiments were conducted in excess of surface sites compared to thiol reactant, the change in mineral structure during aging must be responsible for the observed differences in reactivity with the thiols. These findings indicate that the synthesis of manganese mineral phases plays an important role in reduction kinetics and that great care should be taken to synthesize minerals of appropriate age. Finally, among all the Mn oxides tested, manganite displayed the lowest rate of cysteine oxidation (Figure 6B) as observed for Cr(III) oxidation by manganite relative to cryptomelane and birnessite[10] and for the oxidation of a number of organic contaminants by Mn oxides of different structure.[12] Despite the higher redox potential of manganite compared to δ-

DOI: 10.1021/acs.est.8b03993
Environ. Sci. Technol. 2018, 52, 13202−13211

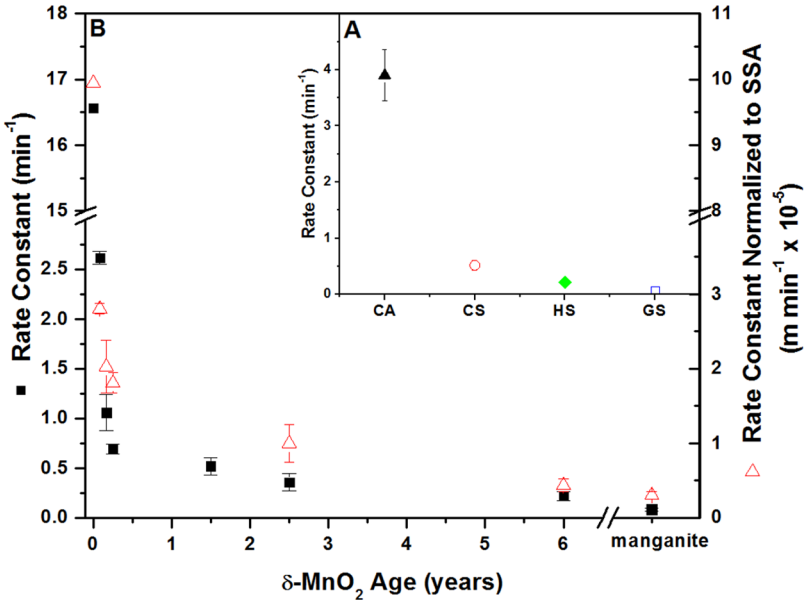

Figure 6. Overall first order rate constants for (A) the reaction of cysteamine (CA), cysteine (CS), homocysteine (HS), and reduced glutathione (GS) with δ-MnO_2 aged for 1.5 years, and (B) the reaction of cysteine with δ-MnO_2 of different age and manganite (left axis, closed black squares) and normalized to BET specific surface area (SSA) (right axis, open red triangles).

MnO_2,[72] slower reaction is likely due to the increased crystallinity as well as the thermodynamic stability of Mn(III) within the MnOOH structure. Indeed, shorter bond lengths with increased orbital overlap are observed between surface Mn(IV) sites of birnessite with inorganic reductants such as arsenite compared to surface Mn(III) sites of manganite.[73] Shorter bond lengths between Mn(IV) and the surface-bound reactant may increase electron transfer and further support increased reduction rates of δ-MnO_2 and even cryptomelane as compared to manganite. Disruption of the mineral structure by formation of surface Mn(III)[71] in the first electron transfer step during Mn(IV) reduction likely decreased the energy necessary for the second electron transfer and increased the rate of thiol oxidation by δ-MnO_2 and cryptomelane as compared to manganite.

4. ENVIRONMENTAL IMPLICATIONS

The findings of this study have important environmental implications. The rapid reduction of an efficient adsorbent and oxidant of inorganic[7−11] and organic[12] contaminants may have important implications on the remediation of environments where thiol production is significant. The differences in reactivity of cysteine with Mn oxides of different structure (i.e., δ-MnO_2 of different age and manganite) also demonstrate the importance of correlating solid phase structure and reactivity when dealing with the redox properties of Mn oxides. In this context, the reaction kinetics of Mn oxides with inorganic and organic reductants should be determined with various δ-MnO_2 transformation products to accurately predict the environmentally relevant biogeochemical significance of Mn oxides in sedimentary environments.

Thiols have been detected in both freshwater[74] and marine[75−78] sediments, and previous studies have demonstrated the importance of cysteine as an electron shuttle during microbial Fe reduction[35,36] and confirmed the reduction of cystine by model metal-reducing bacteria.[35,36,79] The increased abiotic reaction rate between thiols and Mn oxides and the complete conversion of the thiols to their disulfide product compared to the Fe(III) oxide system[38] suggests that thiols may act as electron shuttles during dissimilatory Mn reduction to an even greater extent than during dissimilatory Fe reduction. Thus, if thiols are microbially recycled, even small thiol concentrations may result in significant reduction of Mn oxides in sedimentary environments. The reduction of Mn oxides by thiols may, therefore, have a significant impact on inorganic[7−11] and organic[12] contaminant degradation, indirectly influence the biogeochemical cycling of carbon, nitrogen, phosphorus, sulfur, and iron in sediments,[1−6] and potentially influence interpretation of Mn paleoenvironmental sediment records.[80,81]

■ ASSOCIATED CONTENT

Supporting Information

The Supporting Information is available free of charge on the ACS Publications website at DOI: 10.1021/acs.est.8b03993.

Mn K-edge XAS data collection and analysis; Relative percentage of different Mn oxide mineral phases from linear combination fitting of Mn EXAFS data; BET surface area analysis, results, and rate normalization (PDF)

■ AUTHOR INFORMATION

Corresponding Author

*E-mail: mtaillef@eas.gatech.edu.

ORCID

Yuanzhi Tang: 0000-0002-7741-8646

Martial Taillefert: 0000-0003-2053-6462

Notes

The authors declare no competing financial interest.

■ ACKNOWLEDGMENTS

This work was supported by the National Science Foundation (Grant numbers DEB-1542596 to M.T. and E.E. and CHE-1710285 to Y.T. and S.Z.). We thank Dr. Nadia Szeinbaum for

DOI: 10.1021/acs.est.8b03993
Environ. Sci. Technol. 2018, 52, 13202−13211

synthesis of some Mn oxides, Nan Xie for help with XRD analysis, Biao Wan and Pan Liu for help with EXAFS analyses, and Nathan Ellebracht for BET analysis. We also appreciate the support from beamline scientists Qing Ma (APS 5BM) and Ryan Davis (SSRL 4-1). Finally, we thank three anonymous reviewers and the associate editor for their thoughtful suggestions on an earlier version of this paper. Portions of this research were conducted at the Advanced Photon Source (APS) and Stanford Synchrotron Radiation Lightsource (SSRL). APS is a U.S. Department of Energy (DOE) Office of Science User Facility operated for the DOE Office of Science by Argonne National Laboratory under Contract No. DE-AC02-06CH11357. Use of SSRL, SLAC National Accelerator Laboratory, is supported by DOE Office of Science, Office of Basic Energy Sciences under Contract No. DE-AC02-76SF00515.

REFERENCES

(1) Luther, G. W.; Sundby, B.; Lewis, B. L.; Brendel, P. J.; Silverberg, N. Interactions of manganese with the nitrogen cycle: Alternative pathways to dinitrogen. *Geochim. Cosmochim. Acta* **1997**, *61* (19), 4043−4052.

(2) Burdige, D. J.; Nealson, K. H. Chemical and microbial studies of sulfide-mediated manganese reduction. *Geomicrobiol. J.* **1986**, *4* (4), 361−387.

(3) Schippers, A.; Jorgensen, B. B. Oxidation of pyrite and iron sulfide by manganese dioxide in marine sediments. *Geochim. Cosmochim. Acta* **2001**, *65* (6), 915−922.

(4) Tebo, B. M.; Bargar, J. R.; Clement, B. G.; Dick, G. J.; Murray, K. J.; Parker, D.; Verity, R.; Webb, S. M. Biogenic manganese oxides: Properties and mechanisms of formation. *Annu. Rev. Earth Planet. Sci.* **2004**, *32*, 287−328.

(5) White, D. J.; Noll, M. R.; Makarewicz, J. C. Does Manganese Influence Phosphorus Cycling under Suboxic Lake Water Conditions? *J. Great Lakes Res.* **2008**, *34* (4), 571−580.

(6) Neretin, L. N.; Pohl, C.; Jost, G.; Leipe, T.; Pollehne, F. Manganese cycling in the Gotland Deep, Baltic Sea. *Mar. Chem.* **2003**, *82* (3−4), 125−143.

(7) Nelson, Y. M.; Lion, L. W., Formation of Biogenic Manganese Oxides and Their Influence on the Scavenging of Toxic Trace Elements. In *Geochemical and Hydrological Reactivity of Heavy Metals in Soils*; CRC Press, 2003.

(8) Jenne, E. A. Controls on Mn, Fe, Co, Ni, Cu, and Zn Concentrations in Soils and Water: the Significant Role of Hydrous Mn and Fe Oxides. In *Trace Inorganics In Water*; American Chemical Society, 1968; Vol. 73, pp 337−387.

(9) Feng, X. H.; Zhai, L. M.; Tan, W. F.; Liu, F.; He, J. Z. Adsorption and redox reactions of heavy metals on synthesized Mn oxide minerals. *Environ. Pollut.* **2007**, *147* (2), 366−373.

(10) Weaver, R. M.; Hochella, M. F. The reactivity of seven Mn-oxides with Cr-aq(3+): A comparative analysis of a complex, aq environmentally important redox reaction. *Am. Mineral.* **2003**, *88* (11−12), 2016−2027.

(11) Oscarson, D. W.; Huang, P. M.; Defosse, C.; Herbillon, A. Oxidative power of Mn(IV) and Fe(III) oxides with respect to As(III) in terrestrial and aquatic environments. *Nature* **1981**, *291* (5810), 50−51.

(12) Remucal, C. K.; Ginder-Vogel, M. A critical review of the reactivity of manganese oxides with organic contaminants. *Environ. Sci. Proc. Imp.* **2014**, *16* (6), 1247−66.

(13) Taylor, R.; McKenzie, R.; Norrish, K. The mineralogy and chemistry of manganese in some Australian soils. *Aust. J. Soil Res.* **1964**, *2* (2), 235−248.

(14) Bilinski, H.; Giovanoli, R.; Usui, A.; Hanžel, D. Characterization of Mn oxides in cemented streambed crusts from Pinal Creek, Arizona, U.S.A., and in hot-spring deposits from Yuno-Taki Falls, Hokkaido, Japan. *Am. Mineral.* **2002**, *87* (4), 580−591.

(15) Webb, S.; Tebo, B.; Bargar, J. Structural characterization of biogenic Mn oxides produced in seawater by the marine Bacillus sp. strain SG-1. *Am. Mineral.* **2005**, *90* (8−9), 1342−1357.

(16) Post, J. E. Manganese oxide minerals: Crystal structures and economic and environmental significance. *Proc. Natl. Acad. Sci. U. S. A.* **1999**, *96* (7), 3447−3454.

(17) Parc, S.; Nahon, D.; Tardy, Y.; Vieillard, P. Estimated solubility products and fields of stability for cryptomelane, nsutite, birnessite, and lithiophorite based on natural lateritic weathering sequences. *Am. Mineral.* **1989**, *74* (3−4), 466−475.

(18) Ostwald, J. Genesis and paragenesis of the tetravalent manganese oxides of the australian continent. *Econ. Geol. Bull. Soc. Econ. Geol.* **1992**, *87* (5), 1237−1252.

(19) Lu, A. H.; Li, Y., Reactivity of Natural Mn Oxide Cryptomelane In *Advances in the Environmental Biogeochemistry of Manganese Oxides*; Feng, X.; Li, W.; Zhu, M.; Sparks, D. L., Eds., 2015; Vol. *1197*, pp 89−106.

(20) Faria, G. L.; Reis, E. L.; Jannotti, N.; Araújo, F. G. S. Chemical, physical and typological characterization of main brazilian manganese lump ores. *Lat. Am. Appl. Res.* **2013**, *43*, 17−22.

(21) Anschutz, P.; Dedieu, K.; Desmazes, F.; Chaillou, G. Speciation, oxidation state, and reactivity of particulate manganese in marine sediments. *Chem. Geol.* **2005**, *218* (3−4), 265−279.

(22) van der Zee, C.; van Raaphorst, W. Manganese oxide reactivity in North Sea sediments. *J. Sea Res.* **2004**, *52* (2), 73−85.

(23) Zhu, M.; Ginder-Vogel, M.; Parikh, S. J.; Feng, X.-H.; Sparks, D. L. Cation effects on the layer structure of biogenic Mn-oxides. *Environ. Sci. Technol.* **2010**, *44* (12), 4465−4471.

(24) Zhao, H.; Zhu, M.; Li, W.; Elzinga, E. J.; Villalobos, M.; Liu, F.; Zhang, J.; Feng, X.; Sparks, D. L. Redox Reactions between Mn (II) and Hexagonal Birnessite Change its Layer Symmetry. *Environ. Sci. Technol.* **2016**, *50*, 1750−1758.

(25) Bargar, J. R.; Tebo, B. M.; Bergmann, U.; Webb, S. M.; Glatzel, P.; Chiu, V. Q.; Villalobos, M. Biotic and abiotic products of Mn (II) oxidation by spores of the marine Bacillus sp. strain SG-1. *Am. Mineral.* **2005**, *90* (1), 143−154.

(26) Elzinga, E. J. Reductive transformation of birnessite by aqueous Mn (II). *Environ. Sci. Technol.* **2011**, *45* (15), 6366−6372.

(27) Lefkowitz, J. P.; Rouff, A. A.; Elzinga, E. J. Influence of pH on the reductive transformation of birnessite by aqueous Mn (II). *Environ. Sci. Technol.* **2013**, *47* (18), 10364−10371.

(28) Tu, S.; Racz, G. J.; Goh, T. B. Transformations of synthetic birnessite as affected by pH and manganese concentration. *Clays Clay Miner.* **1994**, *42* (3), 321−330.

(29) Mandernack, K. W.; Post, J.; Tebo, B. M. Manganese mineral formation by bacterial spores of the marine Bacillus, strain SG-1: evidence for the direct oxidation of Mn (II) to Mn (IV). *Geochim. Cosmochim. Acta* **1995**, *59* (21), 4393−4408.

(30) Bargar, J. R.; Fuller, C. C.; Marcus, M. A.; Brearley, A. J.; Perez De la Rosa, M.; Webb, S. M.; Caldwell, W. A. Structural characterization of terrestrial microbial Mn oxides from Pinal Creek, AZ. *Geochim. Cosmochim. Acta* **2009**, *73* (4), 889−910.

(31) Burdige, D. J.; Dhakar, S. P.; Nealson, K. H. Effects of manganese oxide mineralogy on microbial and chemical manganese reduction. *Geomicrobiol. J.* **1992**, *10* (1), 27−48.

(32) Lovley, D. R.; Coates, J. D.; Blunt-Harris, E. L.; Phillips, E. J. P.; Woodward, J. C. Humic substances as electron acceptors for microbial respiration. *Nature* **1996**, *382*, 445.

(33) Coates, J. D.; Cole, K. A.; Chakraborty, R.; O'Connor, S. M.; Achenbach, L. A. Diversity and ubiquity of bacteria capable of utilizing humic substances as electron donors for anaerobic respiration. *Appl. Environ. Microbiol.* **2002**, *68* (5), 2445−52.

(34) Coates, J. D.; Ellis, D. J.; Blunt-Harris, E. L.; Gaw, C. V.; Roden, E. E.; Lovley, D. R. Recovery of humic-reducing bacteria from a diversity of environments. *Appl. Environ. Microbiol.* **1998**, *64* (4), 1504−9.

(35) Doong, R. A.; Schink, B. Cysteine-mediated reductive dissolution of poorly crystalline iron(III) oxides by Geobacter sulfurreducens. *Environ. Sci. Technol.* **2002**, *36* (13), 2939−2945.

DOI: 10.1021/acs.est.8b03993
Environ. Sci. Technol. 2018, 52, 13202−13211

(36) Liu, D.; Dong, H.; Zhao, L.; Wang, H. Smectite Reduction by Shewanella Species as Facilitated by Cystine and Cysteine. *Geomicrobiol. J.* **2014**, *31* (1), 53−63.
(37) Amirbahman, A.; Sigg, L.; vonGunten, U. Reductive dissolution of Fe(III) (hydr)oxides by cysteine: Kinetics and mechanism. *J. Colloid Interface Sci.* **1997**, *194* (1), 194−206.
(38) Eitel, E. M.; Taillefert, M. Mechanistic investigation of Fe(III) oxide reduction by low molecular weight organic sulfur species. *Geochim. Cosmochim. Acta* **2017**, *215*, 173−188.
(39) Andrabi, S. M. Z.; Khan, Z. Reactivity of some sulphur- and non-sulphur-containing amino acids towards water soluble colloidal MnO2. A kinetic study. *Colloid Polym. Sci.* **2007**, *285* (4), 389−396.
(40) Herszage, J.; Afonso, M. D.; Luther, G. W. Oxidation of cysteine and glutathione by soluble polymeric MnO(2). *Environ. Sci. Technol.* **2003**, *37* (15), 3332−3338.
(41) Altaf, M.; Jaganyi, D. Kinetics of the Degradation of l-Cysteine at Freshly Prepared Nano-sized MnO2 Surfaces in the Absence and Presence of TX-100. *J. Solution Chem.* **2014**, *43* (2), 269−282.
(42) Salamon, C. W.; Jameson, R. F.; Linert, W. Anaerobic oxidation of cysteine to cystine by manganese(III) in aqueous acetic acid. *Inorg. Chim. Acta* **2004**, *357* (1), 41−50.
(43) Murray, J. W. Surface chemistry of hydrous manganese-dioxide. *J. Colloid Interface Sci.* **1974**, *46* (3), 357−371.
(44) Deguzman, R. N.; Shen, Y. F.; Neth, E. J.; Suib, S. L.; Oyoung, C. L.; Levine, S.; Newsam, J. M. Sythesis and characterization of ocathedral molecular-sieves (OMS-2) having the hollandite structure. *Chem. Mater.* **1994**, *6* (6), 815−821.
(45) Inman, M. P.; Beattie, J. K.; Jones, D. R.; Baldwin, D. S. Abiotic hydrolysis of the detergent builder tripolyphosphate by hydrous manganese dioxide. *Water Res.* **2001**, *35* (8), 1987−1993.
(46) Moore, T. E.; Ellis, M.; Selwood, P. W. Solid Oxides and Hydroxides of Manganese1. *J. Am. Chem. Soc.* **1950**, *72* (2), 856−866.
(47) Lefkowitz, J. P.; Elzinga, E. J. Impacts of Aqueous Mn(II) on the Sorption of Zn(II) by Hexagonal Birnessite. *Environ. Sci. Technol.* **2015**, *49* (8), 4886−4893.
(48) Myers, C. R.; Nealson, K. H. Bacterial manganese reduction and growth with manganese oxide as the sole electron-acceptor. *Science* **1988**, *240* (4857), 1319−1321.
(49) Luther, G. W., III; Glazer, B. T.; Ma, S.; Trouwborst, R. E.; Moore, T. S.; Metzger, E.; Kraiya, C.; Waite, T. J.; Druschel, G.; Sundby, B.; Taillefert, M.; Nuzzio, D. B.; Shank, T. M.; Lewis, B. L.; Brendel, P. J. Use of voltammetric solid-state (micro)electrodes for studying biogeochemical processes: Laboratory measurements to real time measurements with an in situ electrochemical analyzer (ISEA). *Mar. Chem.* **2008**, *108* (3−4), 221−235.
(50) Brendel, P. J.; Luther, G. W. Development of a gold amalgam voltammetric miroelectrode for the determination of dissolved Fe, Mn, O2, and S(-II) in porewater of marine and fresh-water sediments. *Environ. Sci. Technol.* **1995**, *29* (3), 751−761.
(51) Bristow, G.; Taillefert, M. VOLTINT: A Matlabg (R)-based program for semi-automated processing of geochemical data acquired by voltammetry. *Comput. Geosci.* **2008**, *34* (2), 153−162.
(52) Villalobos, M.; Toner, B.; Bargar, J.; Sposito, G. Characterization of the manganese oxide produced by pseudomonas putida strain MnB1. *Geochim. Cosmochim. Acta* **2003**, *67* (14), 2649−2662.
(53) Hinkle, M. A.; Flynn, E. D.; Catalano, J. G. Structural response of phyllomanganates to wet aging and aqueous Mn (II). *Geochim. Cosmochim. Acta* **2016**, *192*, 220−234.
(54) Lanson, B.; Drits, V. A.; Gaillot, A.-C.; Silvester, E.; Plançon, A.; Manceau, A. Structure of heavy-metal sorbed birnessite: Part 1. Results from X-ray diffraction. *Am. Mineral.* **2002**, *87* (11−12), 1631−1645.
(55) Lanson, B.; Drits, V. A.; Silvester, E.; Manceau, A. Structure of H-exchanged hexagonal birnessite and its mechanism of formation from Na-rich monoclinic buserite at low pH. *Am. Mineral.* **2000**, *85* (5−6), 826−838.
(56) Tang, Y.; Webb, S. M.; Estes, E. R.; Hansel, C. M. Chromium (III) oxidation by biogenic manganese oxides with varying structural ripening. *Environ. Sci. Proc. Imp.* **2014**, *16* (9), 2127−2136.
(57) Learman, D.; Voelker, B.; Vazquez-Rodriguez, A.; Hansel, C. Formation of manganese oxides by bacterially generated superoxide. *Nat. Geosci.* **2011**, *4* (2), 95−98.
(58) Learman, D. R.; Wankel, S. D.; Webb, S. M.; Martinez, N.; Madden, A. S.; Hansel, C. M. Coupled biotic−abiotic Mn(II) oxidation pathway mediates the formation and structural evolution of biogenic Mn oxides. *Geochim. Cosmochim. Acta* **2011**, *75* (20), 6048−6063.
(59) Feng, X. H.; Zhu, M.; Ginder-Vogel, M.; Ni, C.; Parikh, S. J.; Sparks, D. L. Formation of nano-crystalline todorokite from biogenic Mn oxides. *Geochim. Cosmochim. Acta* **2010**, *74* (11), 3232−3245.
(60) Cui, H.; Liu, F.; Feng, X.; Tan, W.; Wang, M. K. Aging promotes todorokite formation from layered manganese oxide at near-surface conditions. *J. Soils Sediments* **2010**, *10* (8), 1540−1547.
(61) Li, Y.-F.; Zhu, S.-C.; Liu, Z.-P. Reaction network of layer-to-tunnel transition of MnO2. *J. Am. Chem. Soc.* **2016**, *138* (16), 5371−5379.
(62) Luther, G. W., The frontier-molecular-orbital theory approach in geotechnical processes. In *Aquatic Chemical Kinetics*; Stumm, W., Ed.; John Wiley & Sons: New York, 1990; p 173.
(63) Stumm, W.; Morgan, J. *Aquatic Chemistry: Chemical Equilibria and Rates in Natural Waters*, 3 ed.; Wiley Interscience: New York, 1996.
(64) Shindo, H.; Huang, P. M. Catalytic effects of manganese(IV), iron(III), aluminum, and silicon-oxides on the formation of phenolic polymers. *Soil Sci. Soc. Am. J.* **1984**, *48* (4), 927−934.
(65) Luther, G. W. Manganese(II) oxidation and Mn(IV) reduction in the environment - Two one-electron transfer steps versus a single two-electron step. *Geomicrobiol. J.* **2005**, *22* (3−4), 195−203.
(66) Banerjee, D.; Nesbitt, H. W. Oxidation of aqueous Cr(III) at birnessite surfaces: Constraints on reaction mechanism. *Geochim. Cosmochim. Acta* **1999**, *63* (11−12), 1671−1687.
(67) Banerjee, D.; Nesbitt, H. W. XPS study of reductive dissolution of birnessite by H2SeO3 with constraints on reaction mechanism. *Am. Mineral.* **2000**, *85* (5−6), 817−825.
(68) Nesbitt, H. W.; Canning, G. W.; Bancroft, G. M. XPS study of reductive dissolution of 7 angstrom-birnessite by H3AsO3, with constraints on reaction mechanism. *Geochim. Cosmochim. Acta* **1998**, *62* (12), 2097−2110.
(69) Lin, H.; Szeinbaum, N. H.; DiChristina, T. J.; Taillefert, M. Microbial Mn(IV) reduction requires an initial one-electron reductive solubilization step. *Geochim. Cosmochim. Acta* **2012**, *99*, 179−192.
(70) Kostka, J. E.; Luther, G. W.; Nealson, K. H. Chemical and biological reduciton of Mn(III)-pyrophosphate complexes - potential importance of dissolved Mn(III) as an environmental oxidant. *Geochim. Cosmochim. Acta* **1995**, *59* (5), 885−894.
(71) Nico, P. S.; Zasoski, R. J. Importance of Mn(III) Availability on the Rate of Cr(III) Oxidation on δ-MnO2. *Environ. Sci. Technol.* **2000**, *34* (16), 3363−3367.
(72) Bricker, O. Some stability relations in system Mn-O2-H2O at 25 degrees and 1 atm total pressure. *Am. Mineral.* **1965**, *50* (9), 1296.
(73) Zhu, M.; Paul, K. W.; Kubicki, J. D.; Sparks, D. L. Quantum Chemical Study of Arsenic (III, V) Adsorption on Mn-Oxides: Implications for Arsenic(III) Oxidation. *Environ. Sci. Technol.* **2009**, *43* (17), 6655−6661.
(74) Zhang, J.; Wang, F.; House, J. D.; Page, B. Thiols in wetland interstitial waters and their role in mercury and methylmercury speciation. *Limnol. Oceanogr.* **2004**, *49* (6), 2276−2286.
(75) Kiene, R. P. Evidence for the biological turnover of thiols in anoxic marine sediments. *Biogeochemistry* **1991**, *13* (2), 117−135.
(76) Luther, G. W.; Church, T. M.; Scudlark, J. R.; Cosman, M. Inorganic and Organic Sulfur Cycling in Salt-Marsh Pore Waters. *Science* **1986**, *232* (4751), 746−749.
(77) Kiene, R. P.; Taylor, B. F. Demethylation of Dimethylsulfoniopropionate and Production of Thiols in Anoxic Marine Sediments. *Appl. Environ. Microbiol.* **1988**, *54* (9), 2208−2212.
(78) MacCrehan, W.; Shea, D., Temporal relationship of thiols to inorganic sulfur compounds in anoxic Chesapeake Bay sediment porewater. In *Geochemical Transformations of Sedimentary Sulfur*;

DOI: 10.1021/acs.est.8b03993
Environ. Sci. Technol. 2018, 52, 13202−13211

Vairavamurthy, M. A., Schoonen, M. A. A., Eds.; 1995; Vol. *612*, pp 294−310.
(79) Kaden, J.; Galushko, A. S.; Schink, B. Cysteine-mediated electron transfer in syntrophic acetate oxidation by cocultures of Geobacter sulfurreducens and Wolinella succinogenes. *Arch. Microbiol.* **2002**, *178* (1), 53−58.
(80) Johnson, J. E.; Webb, S. M.; Ma, C.; Fischer, W. W. Manganese mineralogy and diagenesis in the sedimentary rock record. *Geochim. Cosmochim. Acta* **2016**, *173*, 210−231.
(81) Maynard, J. B. The chemistry of manganese ores through time: A signal of increasing diversity of earth-surface environments. *Econ. Geol. Bull. Soc. Econ. Geol.* **2010**, *105* (3), 535−552.

DOI: 10.1021/acs.est.8b03993
Environ. Sci. Technol. 2018, 52, 13202−13211